Supplementary Information

A photoswitchable tetra-azo macrocycle enabling light-controlled host-in-host binding and release of cucurbit[5]uril

Yue Wu‡, Kuirong Fu‡, Song Qin, Ming Ouyang, Zhiyao Yang, Yimin Cai, Wen Feng, Lihua Yuan*, and Xiaowei Li*

College of Chemistry, Key Laboratory of Radiation Physics and Technology of Ministry of Education, Institute of Nuclear Science and Technology, Sichuan University, Chengdu, 610064, China

‡ These authors contributed equally to this work.

E-mails: lhyuan@scu.edu.cn, lixw@scu.edu.cn

Table of Contents

1. Materials and Methods

1.1 Reactions and Purifications

All chemicals were purchased from commercial suppliers and used without further purification unless otherwise stated. Column chromatography was performed on silica gel (100-200 mesh or 300–400 mesh). Reaction progress was monitored by thin-layer chromatography (TLC). Solvents used for extraction and chromatography were of reagent grade.

1.2 Characterizations

Nuclear Magnetic Resonance (NMR) Spectroscopy

NMR spectra were recorded on Bruker AVANCE AV II-400 MHz spectrometers operating at 400 or 600 MHz for ^{1}H and 100 MHz for ^{13}C at 298 K. Deuterated solvents, e.g. $CDCl_3$ and CD_3CN, were obtained from Cambridge Isotope Laboratories. Chemical shifts (δ) are reported in ppm using tetramethylsilane (TMS) or residual solvent as the internal standard, and coupling constants (*J*) are denoted in hertz (Hz). Signal multiplicities are denoted as s = singlet, d = doublet, t = triplet, dd = double doublet, m = multiples. Two-dimensional DOSY and NOESY NMR spectra were recorded on a Bruker AVANCE AV II-400 MHz spectrometer at 298 K using a mixing time of 0.4 s.

Isomerization Experiments Monitored by ^{1}H NMR:

Unless otherwise noted, all isomerization experiments were conducted at a concentration of 2 mM. Samples were irradiated using fluorescent lamps (3 W, 365 nm UV lamp or 3 W, 455 nm blue lamp) positioned 20 cm from the NMR tubes. ^{1}H NMR spectra were recorded after irradiation for specified time intervals.

Ultraviolet–Visible (UV–Vis) Spectroscopy

UV–vis absorption spectra were recorded on a Shimadzu UV-2600i spectrophotometer. Unless otherwise specified, measurements were performed in HPLC-grade chloroform.

Matrix-Assisted Laser Desorption/Ionization Time-of-Flight Mass Spectrometry (MALDI-TOF MS)

MALDI-TOF MS spectra were acquired on a Bruker UltrafleXtreme instrument using 2,5-dihydroxybenzoic acid (DHB) as the matrix. The analyzer was operated at an acceleration voltage of +20 kV, with the laser focused using an 8.02 kV lens. Pulsed ion extraction was optimized to 170 ns. For each sample, spectra were collected from 10 distinct deposition spots, with a total of 500 laser shots accumulated.

Single-Crystal X-ray Diffraction

Single-crystal X-ray diffraction data were collected on an Xcalibur E diffractometer using graphite-monochromated Cu K_α radiation (λ = 1.54184 Å). Detailed crystallographic data, including data collection and structure refinement parameters, are provided in the corresponding CIF files and are available free of charge from the Cambridge Crystallographic Data Centre (CCDC). https://www.ccdc.cam.ac.uk/.

2. Synthesis and characterizations

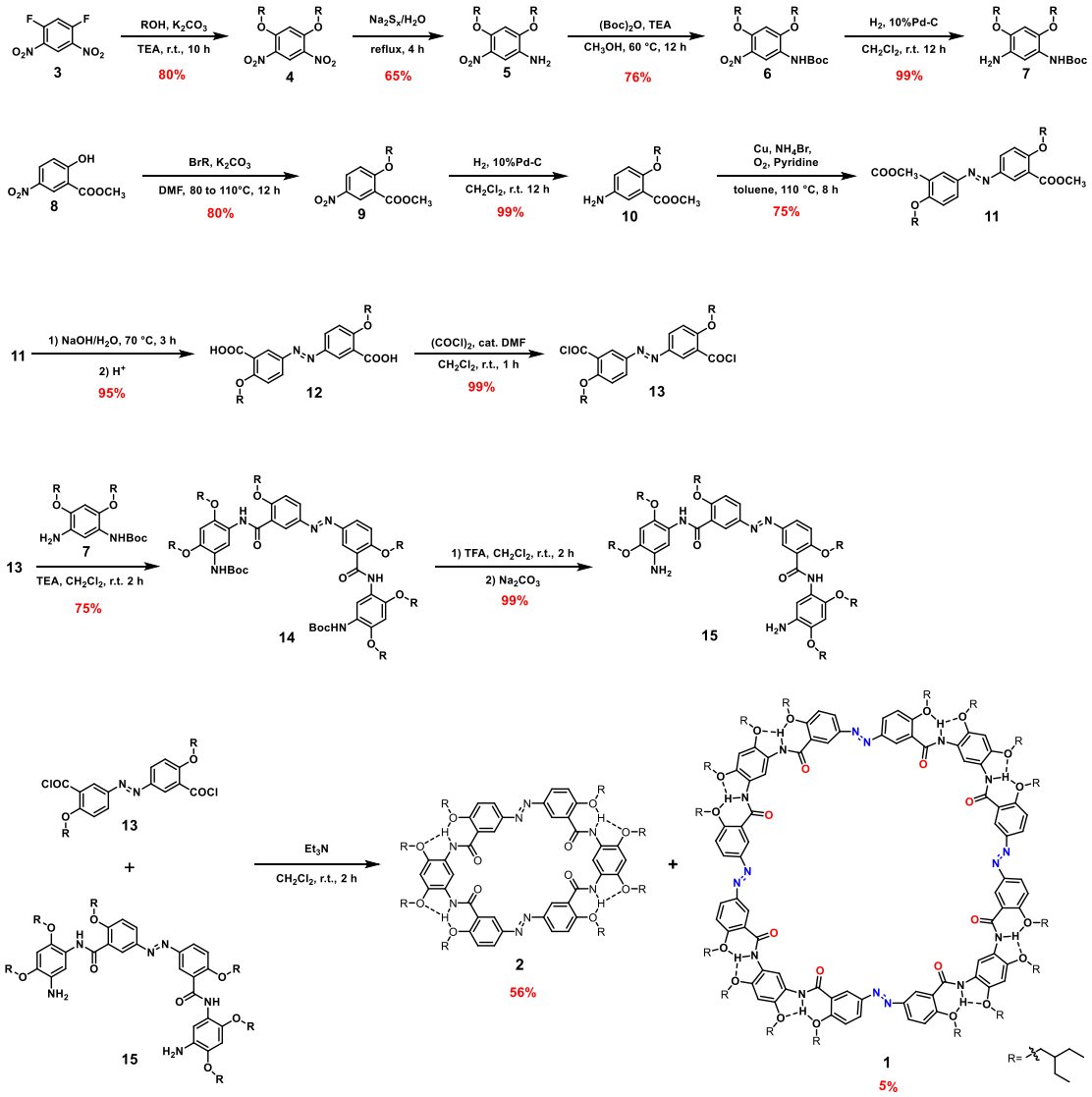

Scheme S1 Synthetic route of macrocycle **1**.

Compounds **4**-**15** are known compounds and were synthesized according to previously reported procedures.[1]

2.1 Synthesis of macrocycle 1

A solution of compound **13** (1.05 equiv.) in dichloromethane (DCM, 30 mL) was added dropwise to a stirred solution of compound **15** (1.0 equiv.) and triethylamine (Et_3N, 4.0 equiv.) in DCM (200 mL) at 0 °C under a nitrogen atmosphere. The reaction mixture was stirred for 5 h under N_2. After completion, the reaction mixture was washed with water (3 × 50 mL), and the organic layer was dried over anhydrous Na_2SO_4. Removal of the solvent under reduced pressure afforded a yellow residue, which was dissolved in a minimal amount of DCM. Addition of excess acetone induced precipitation of macrocycle **1** as a yellow solid (87 mg, 5%).^{1}H NMR (400 MHz, $CDCl_3$, 298 K): δ 9.57 (s, 8H), 9.08 (s, 4H), 8.88 (d, *J* = 2.6 Hz, 8H), 8.03 (dd, *J* = 8.8, 2.7 Hz, 8H), 7.14 (d, *J* = 8.9 Hz, 8H),

6.60 (s, 4H), 4.15 (d, *J* = 6.3 Hz, 16H), 3.92 (d, *J* = 6.2 Hz, 16H), 1.89 (h, *J* = 6.2 Hz, 8H), 1.77-1.68 (m, 8H), 1.57-1.33 (m, 64H), 0.91 (m, *J* = 15.0, 7.4 Hz, 96H). ^{13}C NMR (101 MHz, $CDCl_3$): δ 162.69, 158.62, 147.41, 146.92, 128.45, 123.66, 120.85, 113.01, 72.40, 71.97, 40.81, 40.26, 23.20, 23.14, 11.03, 10.87. ESI-HRMS m/z calculated for $C_{176}H_{248}N_{16}O_{24}$ $[M+3H]^{3+}$ 990.6693, found 991.2975.

2.2 Characterizations

NMR Spectra

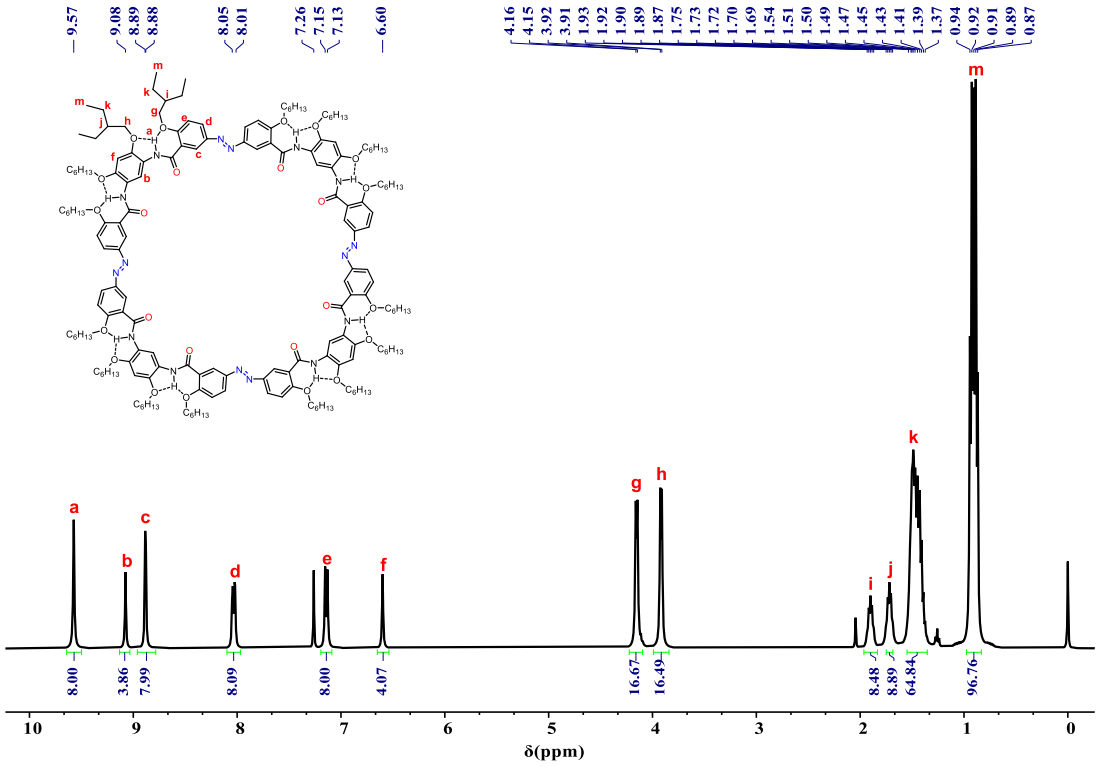

Figure S1. ^{1}H NMR spectrum (2 mM, $CDCl_3$, 400 MHz, 298 K,) of macrocycle **1**.

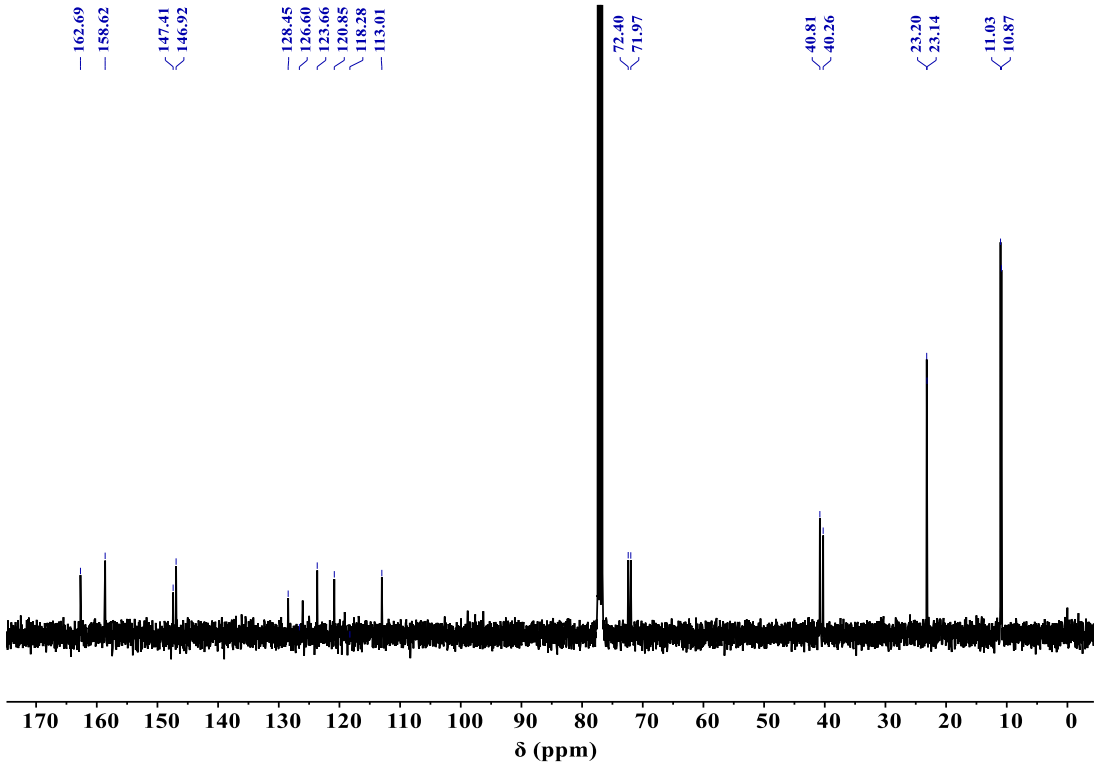

Figure S2. ^{13}C NMR spectrum (10 mM, $CDCl_3$, 101 MHz, 298 K) of macrocycle **1**.

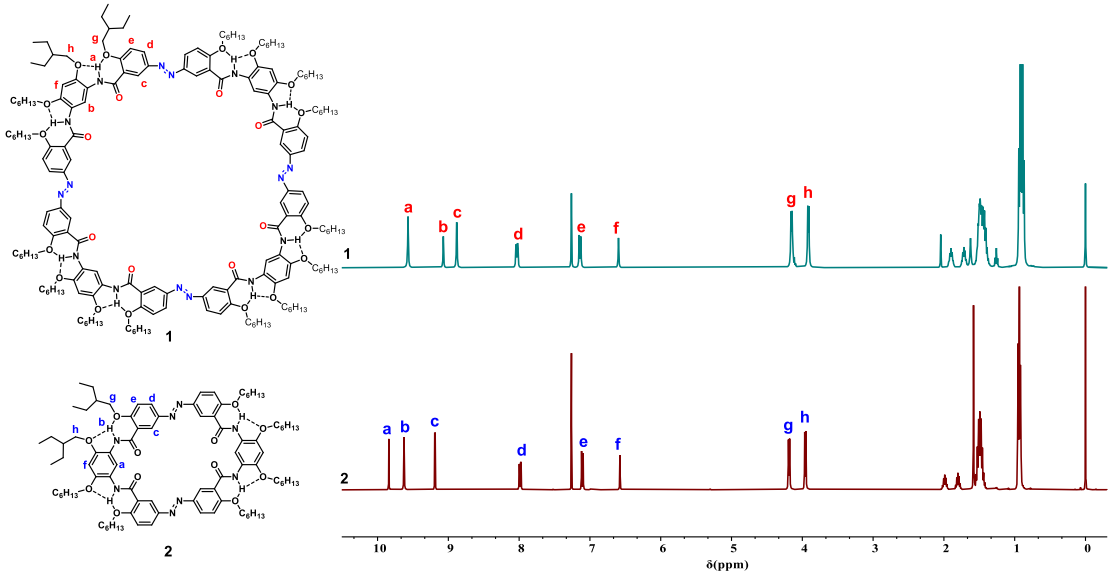

Figure S3. Stacked ^{1}H NMR spectrum (2 mM, $CDCl_3$, 400 MHz, 298 K) of macrocycle **1** and **2**.

2D NOESY Spectrum

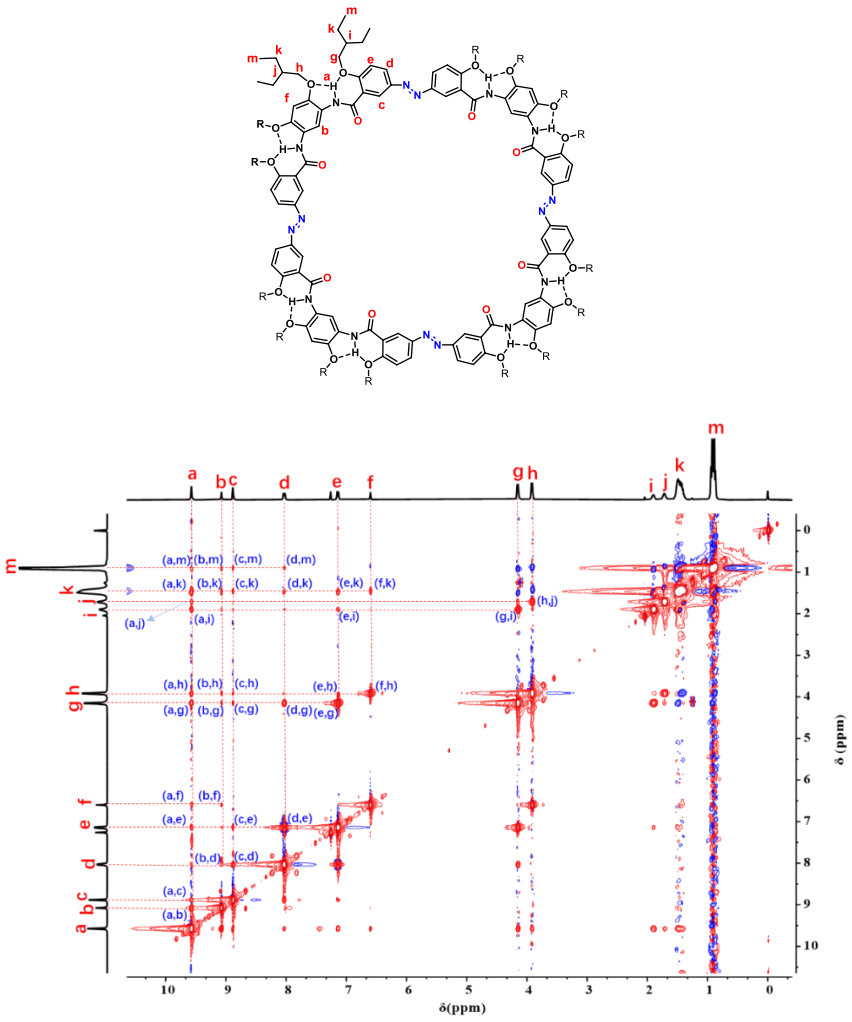

Figure S4. Expanded 2D NOESY spectrum of macrocycle **1** (10 mM, 400 MHz, $CDCl_3$, 298 K, mixing time=0.4 s).

2D ROESY Spectrum

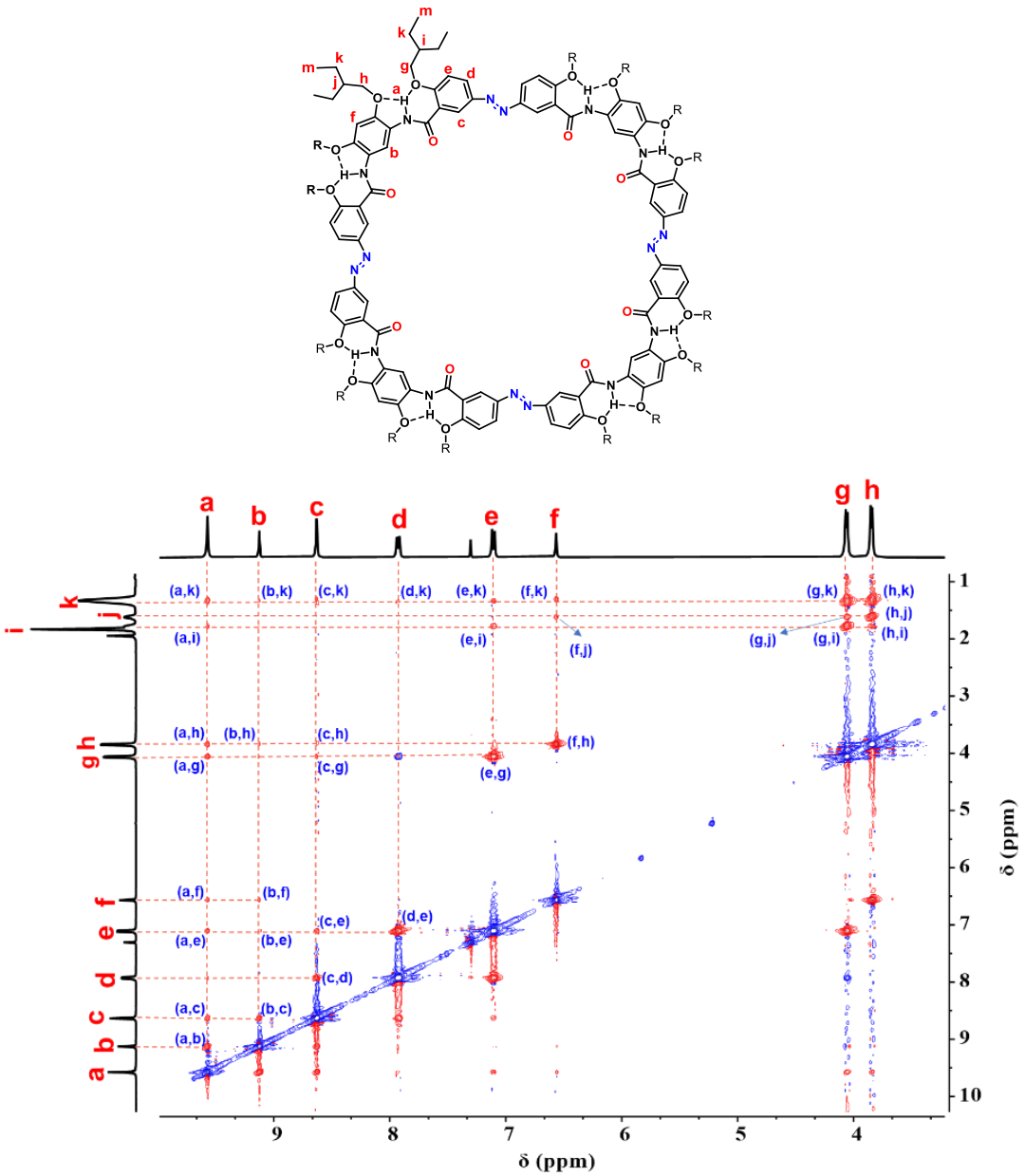

Figure S5. Expanded 2D ROESY spectrum of macrocycle **1** (10 mM, 400 MHz, $CDCl_3/CD_3CN$, 2:1, v/v, 298 K, mixing time=0.4 s).

MALDI-TOF Mass Spectrum

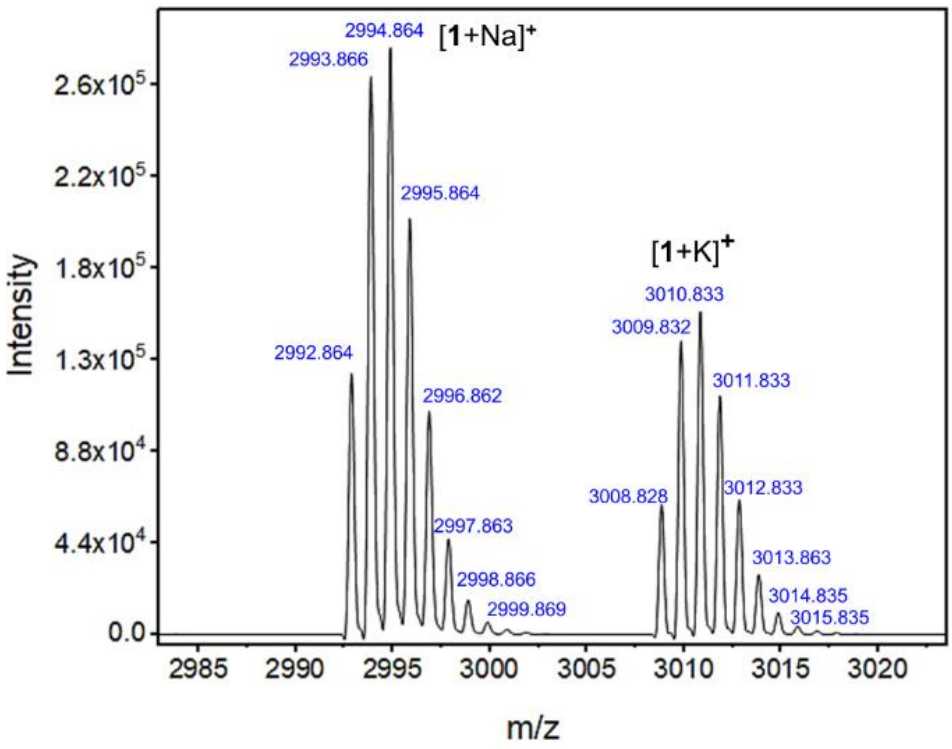

Figure S6. MALDI-TOF MS spectrum of macrocycle **1**.

2.3 Solid State Structure of Macrocycle 1

Single crystals of macrocycle **1** suitable for X-ray diffraction were obtained by vapor diffusion using a mixed solvent system of chloroform and diisopropyl ether. Crystallographic data for **1** have been deposited with the Cambridge Crystallographic Data Centre (CCDC) as supplementary publication **CCDC 2518798**. Full details of data collection and structure refinement are provided in the corresponding CIF files and are available free of charge from the CCDC website www.ccdc.cam.ac.uk/data_request/cif.

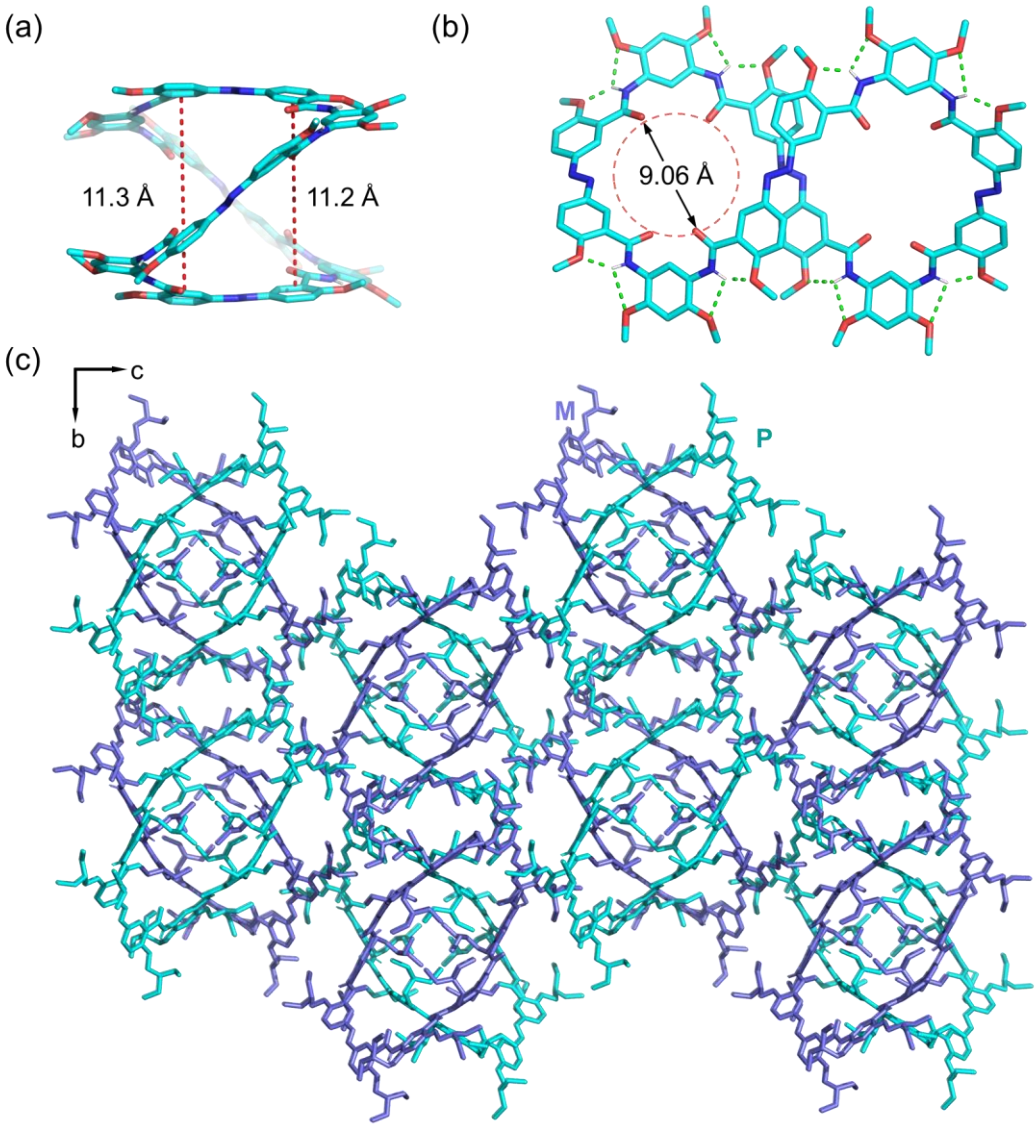

Figure S7. X-ray crystal structure of macrocycle **1**. (a) Side view, with red dotted lines indicating the helical height (Å). (b) Top view, with dashed lines highlighting eight sets of intramolecular three-center hydrogen bonds that stabilize the helical conformation. (c) Side-on view of the 2 × 2 × 2 crystal packing of **1** along the *a* axis. Solvent molecules, side chains, and nonpolar hydrogen atoms have been omitted for clarity.

Table S1. Intramolecular three-center hydrogen bonds parameters observed X-ray crystal structure of macrocycle **1**.

D—H···A	H···A/Å	D···A/Å	D—H···A/˚
N(3)-H(3A)···O(1)	1.912	2.631	137.69
N(3)-H(3A)···O(3)	2.310	2.651	103.04
N(4)-H(4B)···O(4)	2.319	2.669	103.73
N(4)-H(4B)···O(6)	1.960	2.674	137.34
N(7)-H(7)···O(7)	2.216	2.751	127.58
N(7)-H(7)···O(9)	2.305	2.655	103.75
N(8)-H(8A)···O(10)	2.490	2.646	90.37
N(8)-H(8A)···O(12)	1.907	2.633	138.67
N(11)-H(11)···O(13)	1.933	2.658	138.52
N(11)-H(11)···O(15)	2.467	2.680	94.24
N(12)-H(12)···O(16)	2.319	2.565	109.08
N(12)-H(12)···O(18)	1.975	2.692	137.73
N(15)-H(15)···O(19)	2.079	2.724	129.38
N(15)-H(15)···O(21)	2.319	2.667	103.60
N(16)-H(16K)···O(22)	2.510	2.654	89.61
N(16)-H(16K)···O(24)	1.902	2.623	138.15
C(19)-H(19)···O(2)	2.333	2.858	114.32
C(19)-H(19)···O(5A)	2.111	2.742	122.61
C(63)-H(63)···O(8)	2.291	2.855	117.30
C(63)-H(63)···O(11)	2.635	2.982	102.06
C(107)-H(107)···O(14)	2.314	2.813	112.07
C(107)-H(107)···O(17)	2.244	2.853	121.14
C(151)-H(151)···O(20)	2.294	2.846	116.30
C(151)-H(151)···O(23)	2.670	2.999	100.90

Table S2. Crystallographic data of **1**.

Compound	**1**
CCDC	2518798
Empirical formula	$C_{176}H_{248}N_{16}O_{24}$
Formula weight	2972.01
Temperature/K	99.99(10)
Crystal system	orthorhombic
Space group	$Pna2_1$
a/Å	19.9118(2)
b/Å	22.9284(3)
c/Å	40.5812(4)
α/°	90
β/°	90
γ/°	90
Volume/Å^3	18527.2(4)
Z	4
ρ_{calc}g/cm^3	1.279
μ/mm^{-1}	2.593
F(000)	7592.0
Crystal size/mm^3	0.2 × 0.2 × 0.2
Radiation	Cu Kα (λ = 1.54184)
2θ range for data collection/°	4.354 to 151.886
Index ranges	-24≤h≤25, -28≤k≤28, -50≤l≤39
Reflections collected	102474
Independent reflections	28951 [R_{int} = 0.0361, R_{sigma} = 0.0343]
Data/restraints/parameters	28951/2482/2950
Goodness-of-fit on F^2	1.068
Final R indexes [I>=2σ (I)]	R_1 = 0.1116, wR_2 = 0.3155
Final R indexes [all data]	R_1 = 0.1211, wR_2 = 0.3383
Largest diff. peak/hole/e Å^{-3}	1.36/-0.62
Flack parameter	0.506(8)

3. Photoisomerization Studies

3.1 Electronic Absorption Spectroscopy

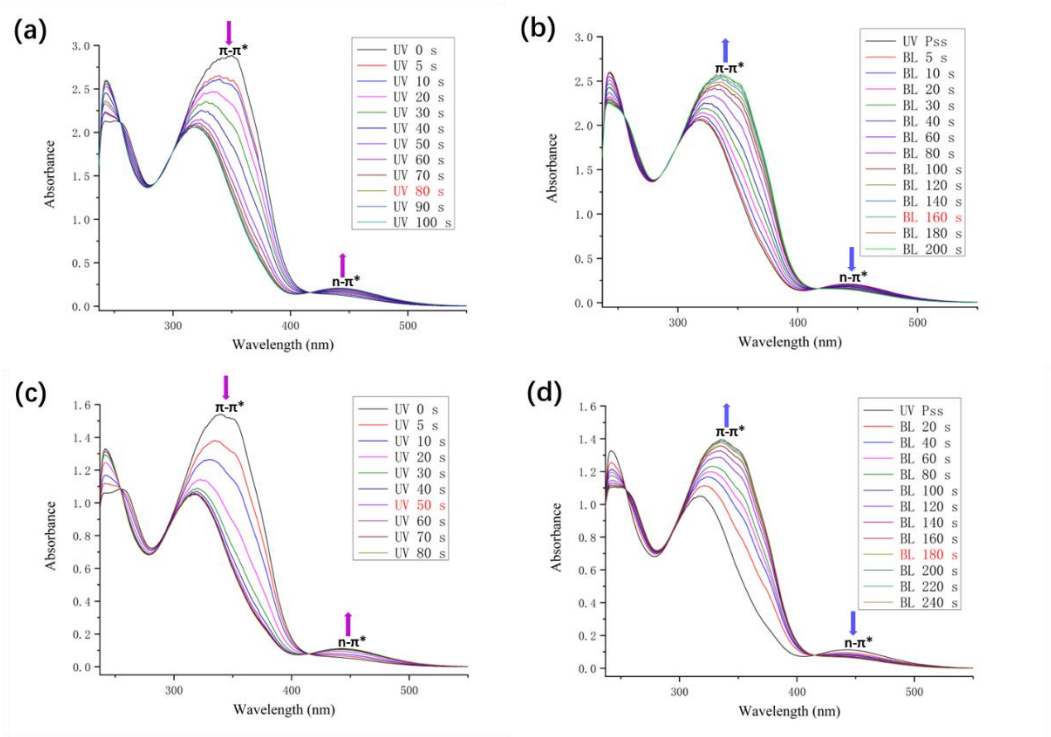

Figure S8. UV-vis absorption spectra (20 µM in $CHCl_3$, 298 K) of macrocycle **1** and macrocycle **2** (a) Spectrum of macrocycle **1** recorded upon increasing UV irradiation at 365 nm for up to 80 s to reach the -*Z* photostationary state (PSS); (b) subsequent irradiation with blue light (450 nm) for 160 s to regenerate the -*E* photostationary state; (c) spectrum of macrocycle **2** recorded upon increasing UV irradiation at 365 nm for up to 50 s to reach the -*Z* photostationary state; (d) subsequent irradiation with blue light (450 nm) for 180 s to regenerate the -*E* photostationary state.

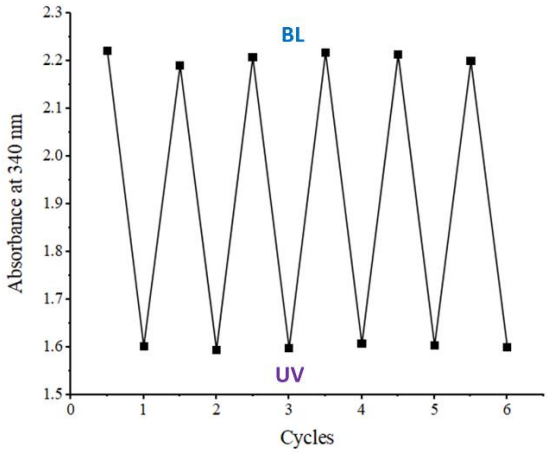

Figure S9. Changes of absorbance at 340 nm for macrocycle **1** (20 µM in $CHCl_3$, 298 K) upon alternating irradiation with UV light and blue light (BL).

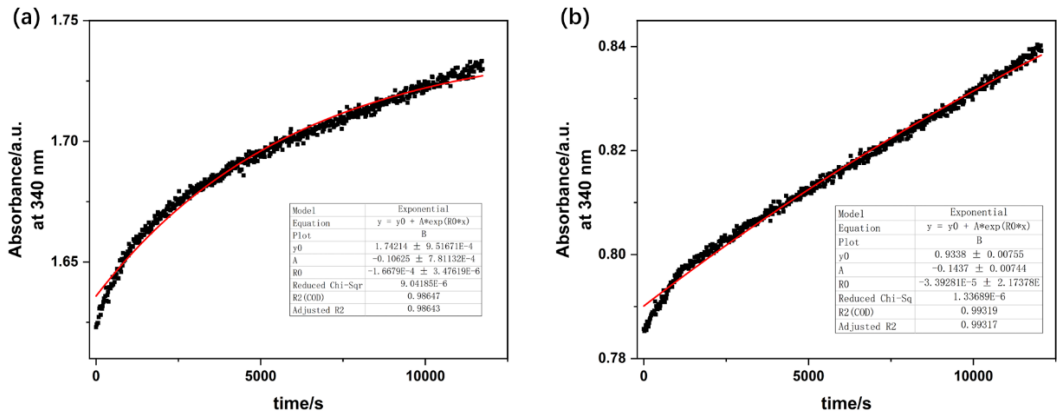

Figure S10. Time-resolved isomerization measurements of (a) macrocycle **1** and (b) macrocycle **2**. Changes in absorbance at 340 nm (black, sampled every 20 s) were monitored over time under dark conditions (20 μM in $CHCl_3$, 298 K). The data were fitted (red) using a first-order rate equation to obtain the average isomerization rate constants. For macrocycle **1**, $k = (1.67 \pm 0.035) \times 10^{-4}$ s^{-1} ($R^2 = 0.986$); for macrocycle **2**, $k = (3.39 \pm 0.22) \times 10^{-5}$ s^{-1} ($R^2 = 0.993$).

3.2 Nuclear Magnetic Resonance Spectroscopy

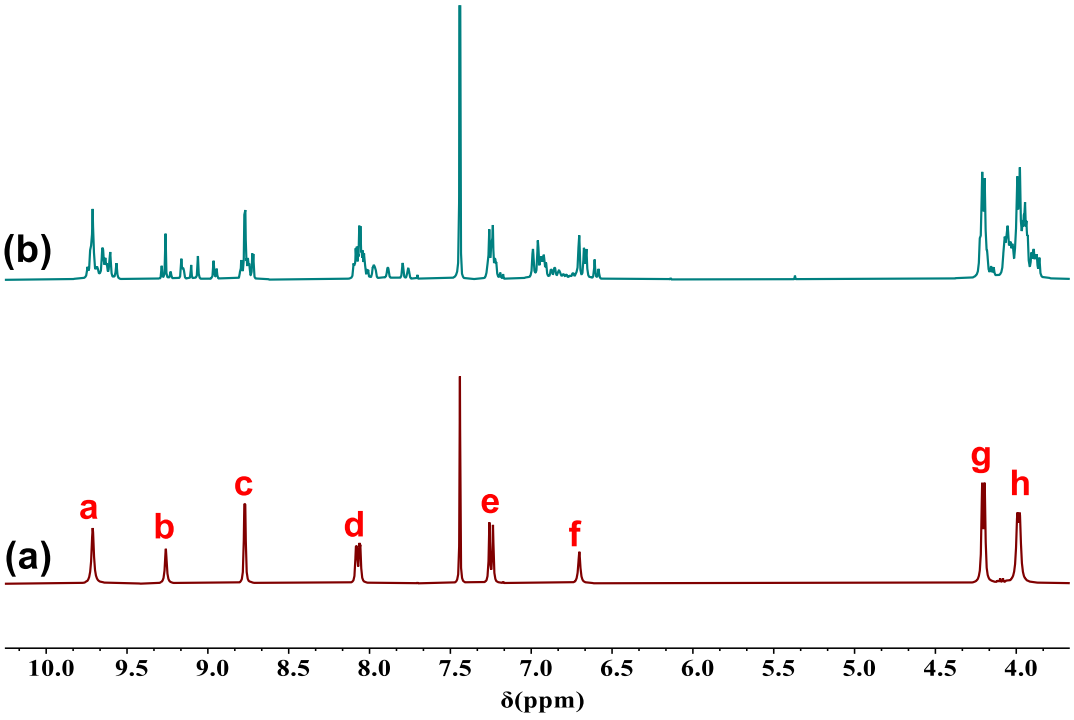

Figure S11. Partial stacked ^1H NMR spectra (2 mM, $CDCl_3/CD_3CN$, 2:1, v/v, 400 MHz, 298 K) illustrating the photoisomerization of macrocycle **1** (a) before irradiation and (b) after irradiation with UV light (365 nm, 3 W) for 1 h.

3.3 DFT Calculation Studies

Density functional theory (DFT) calculations were performed using the Gaussian 09 program. Geometry optimizations of all minima and intermediates were carried out using the Becke three-parameter hybrid functional (B3LYP)[2] and the 6-31G(d)/6-311G(d,p) basis set for C, H, N, and O atoms.

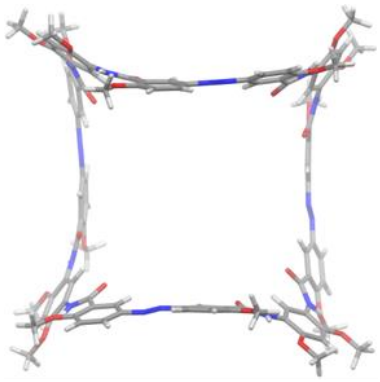

Figure S12. Geometry-optimized molecular structure (B3LYP/6-31G(d) level of theory) of *E,E,E,E*-**1**. All peripheral R^1 groups are replaced by CH_3 for simplicity.

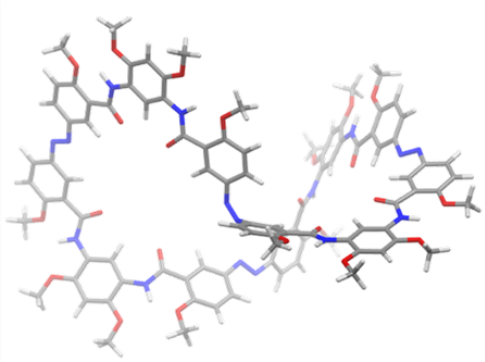

Figure S13. Geometry-optimized molecular structure (B3LYP/6-31G(d) level of theory) of *Z,E,E,E*-**1**. All peripheral R^1 groups are replaced by CH_3 for simplicity.

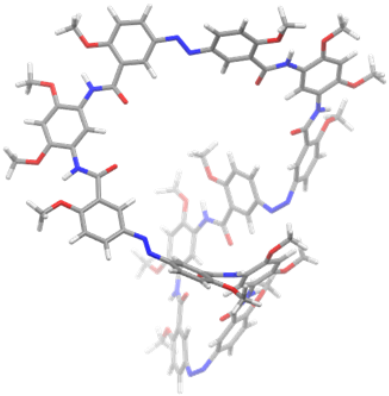

Figure S14. Geometry-optimized molecular structure (B3LYP/6-31G(d) level of theory) of *Z,Z,E,E*-**1**. All peripheral R^1 groups are replaced by CH_3 for simplicity.

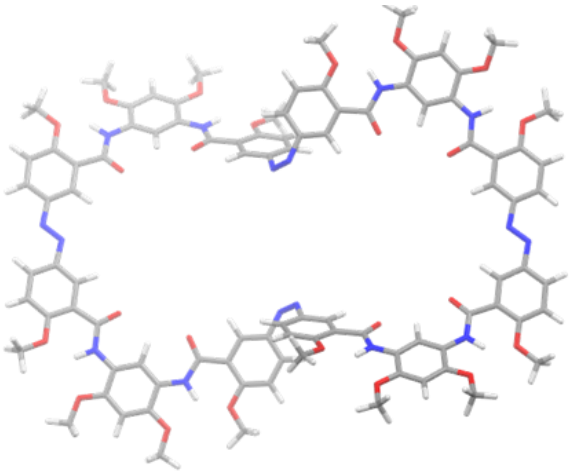

Figure S15. Geometry-optimized molecular structure (B3LYP/6-31G(d) level of theory) of *Z,E,Z,E*-**1**. All peripheral R^1 groups are replaced by CH_3 for simplicity.

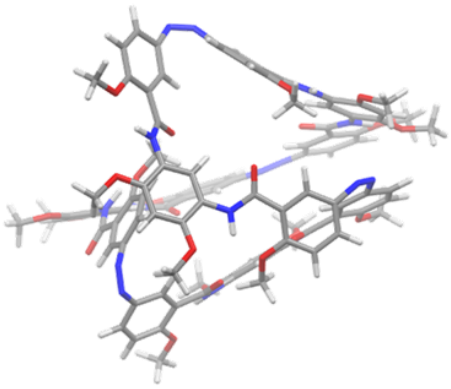

Figure S16. Geometry-optimized molecular structure (B3LYP/6-31G(d) level of theory) of *Z,Z,Z,E*-**1**. All peripheral R^1 groups are replaced by CH_3 for simplicity.

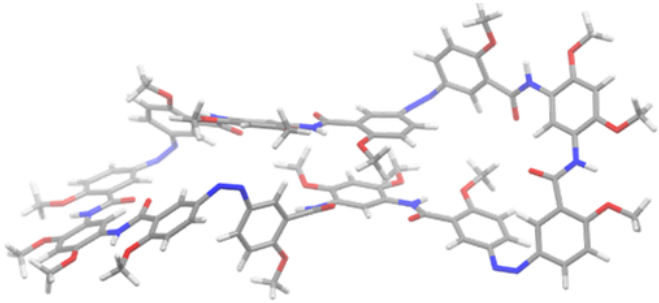

Figure S17. Geometry-optimized molecular structure (B3LYP/6-31G(d) level of theory) of *Z,Z,Z,Z*-**1**. All peripheral R^1 groups are replaced by CH_3 for simplicity.

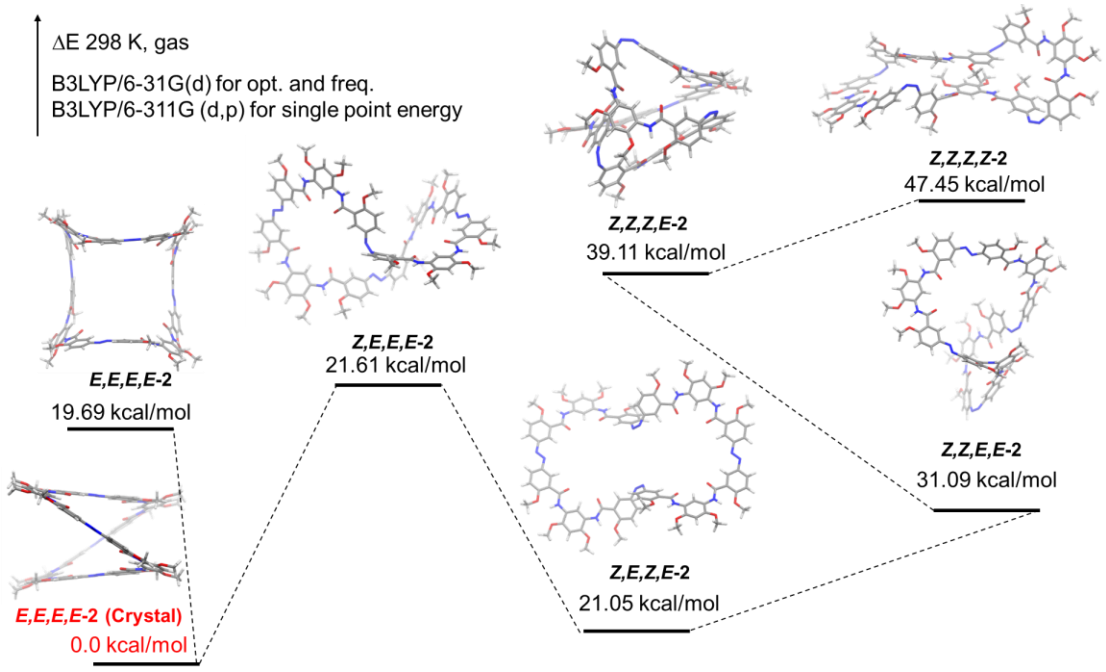

Figure S18. Optimized structures and relative energies of the six stereoisomers of **1**. Energies are reported in kcal mol^{-1} relative to the lowest-energy conformation, *E,E,E,E*-**1** (crystal structure), which is defined as 0 kcal mol^{-1}.

4. Host-Guest Chemistry Studies

4.1 DFT Calculations for H-G Complexes

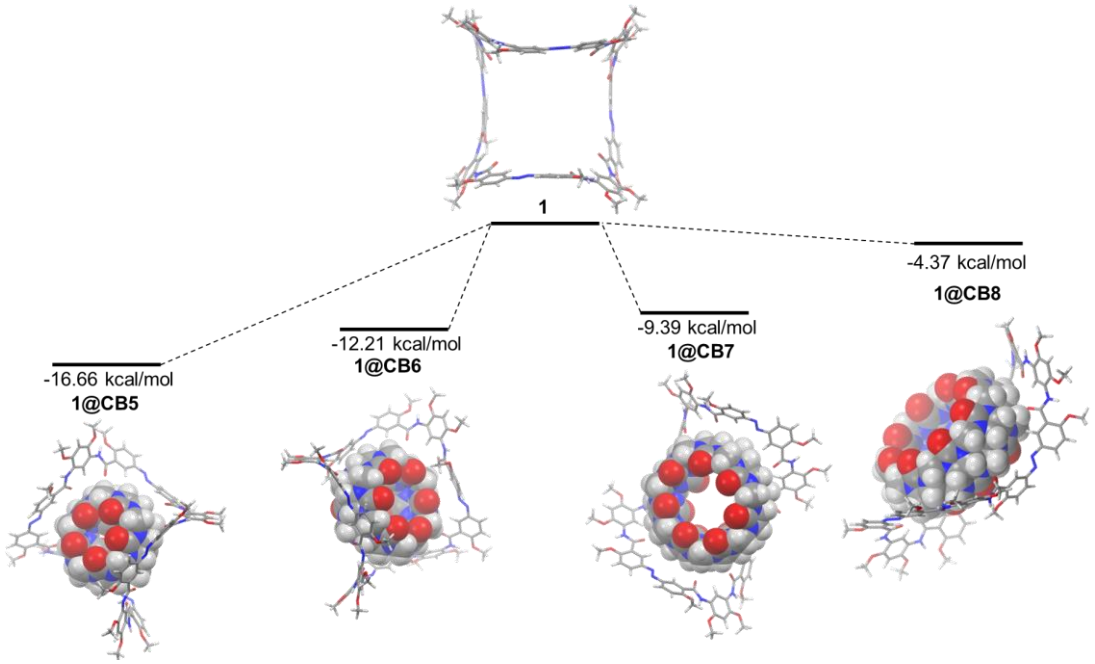

Figure S19. DFT-optimized structures of complexes **1@**CB[n] (*n* = 5-8) at the B3LYP/6-31G(d,p) level of theory. For clarity, all peripheral R groups were replaced by CH_3 groups.

4.2 NMR Spectra for H-G Interactions

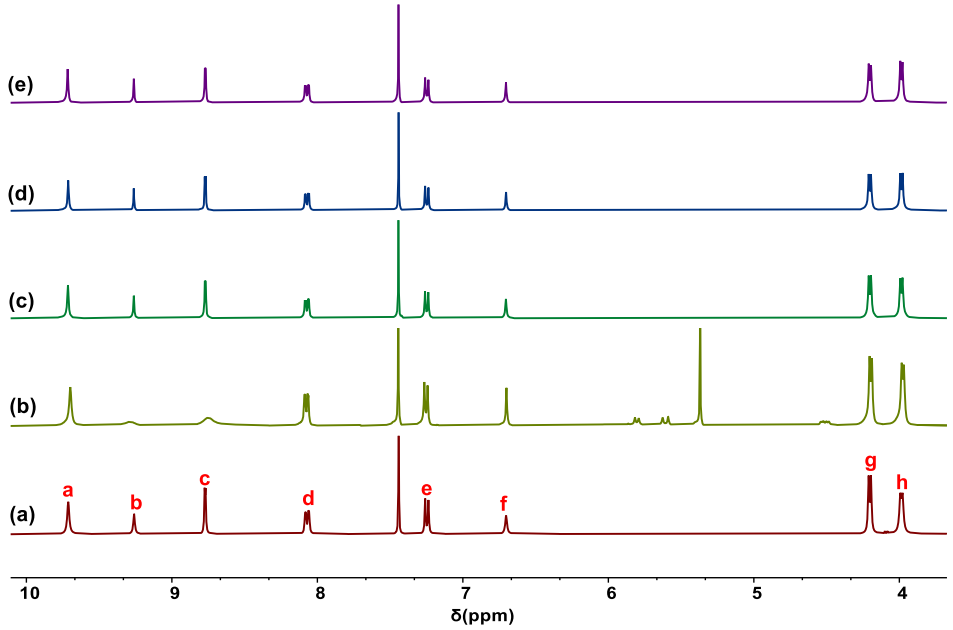

Figure S20. Partial ^{1}H NMR spectra (2 mM in $CDCl_3/CD_3CN$, 2:1, v/v, 400 MHz; 298 K) of (a) macrocycle **1**, (b) **1** with excess CB[5], (c) **1** with excess CB[6], (d) **1** with excess CB[7], and (e) **1** with excess CB[8].

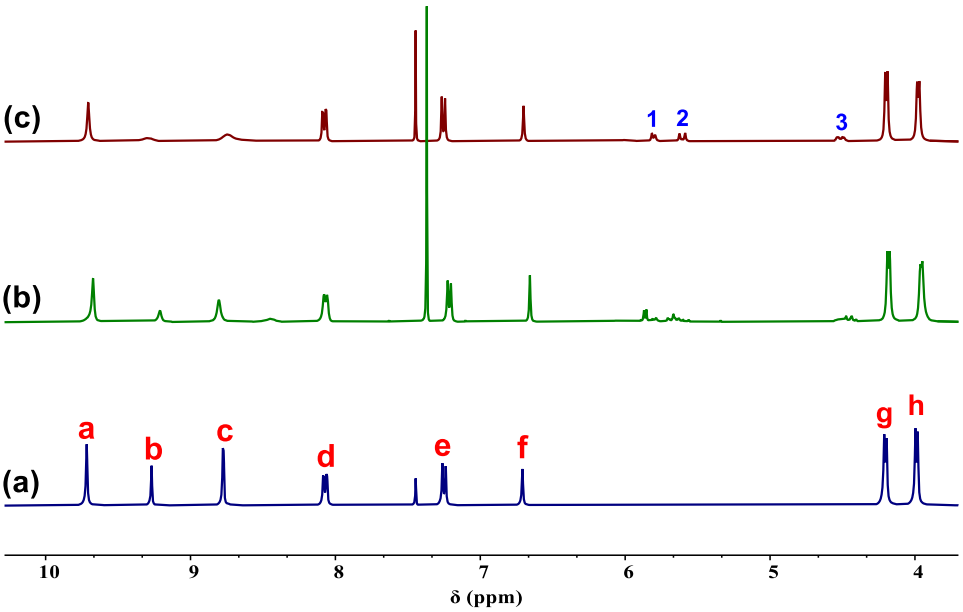

Figure S21. Partial ^{1}H NMR spectra (2 mM, 400 MHz, 298 K) of macrocycle **1** and excess CB[5] (a) $CDCl_3$, (b) $CDCl_3/CD_3CN$, 5:1, v/v, (c) $CDCl_3/CD_3CN$, 2:1, v/v.

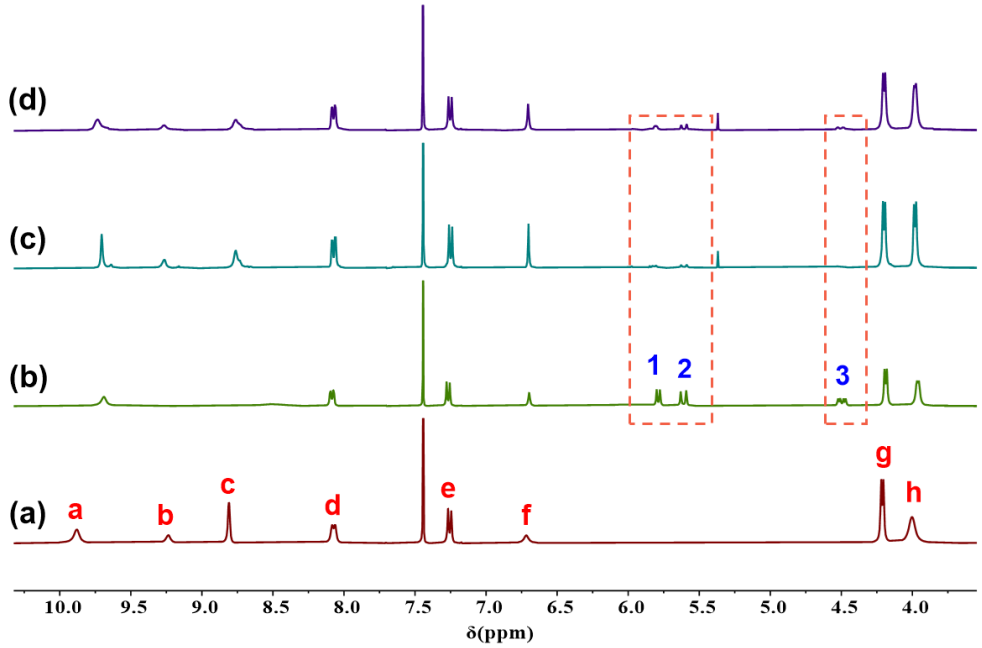

Figure S22. Partial ^{1}H NMR spectra (400 MHz; 298 K, $CDCl_3/CD_3CN$, 2:1 v/v, [**1**] = 2 mM) of macrocycle **1** with (a) 2 equiv. $NaClO_4$, (b) excess CB[5] in the presence of 2 equiv. $NaClO_4$, (c) an equimolar mixture of CB[5]/CB[6]/CB[7]/CB[8] (1:1:1:1 in mole ratio), (d) an equimolar mixture of CB[5]/CB[6]/CB[7]/CB[8] (1:1:1:1 in mole ratio) in the presence of 2 equiv. $NaClO_4$.

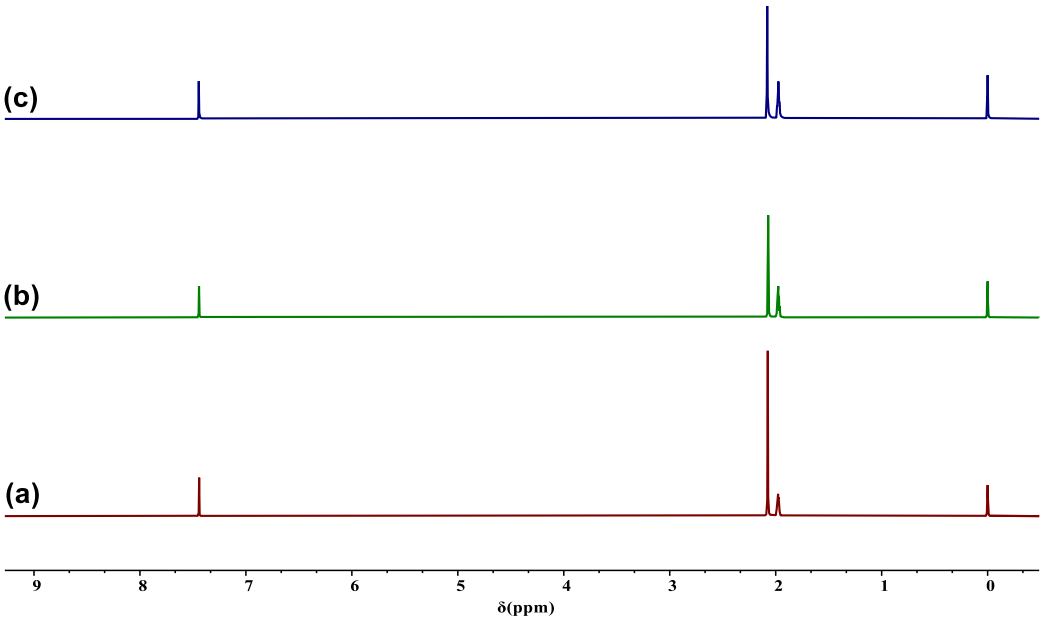

Figure S23. ^{1}H NMR spectra ($CDCl_3/CD_3CN$, 2:1 v/v, 400 MHz, 298 K) of (a) CB[5], (b) CB[5] in the presence of 2 mM $NaClO_4$, and (c) CB[5] in the presence of 4 mM $NaClO_4$.

2D NOESY for H-G Interactions

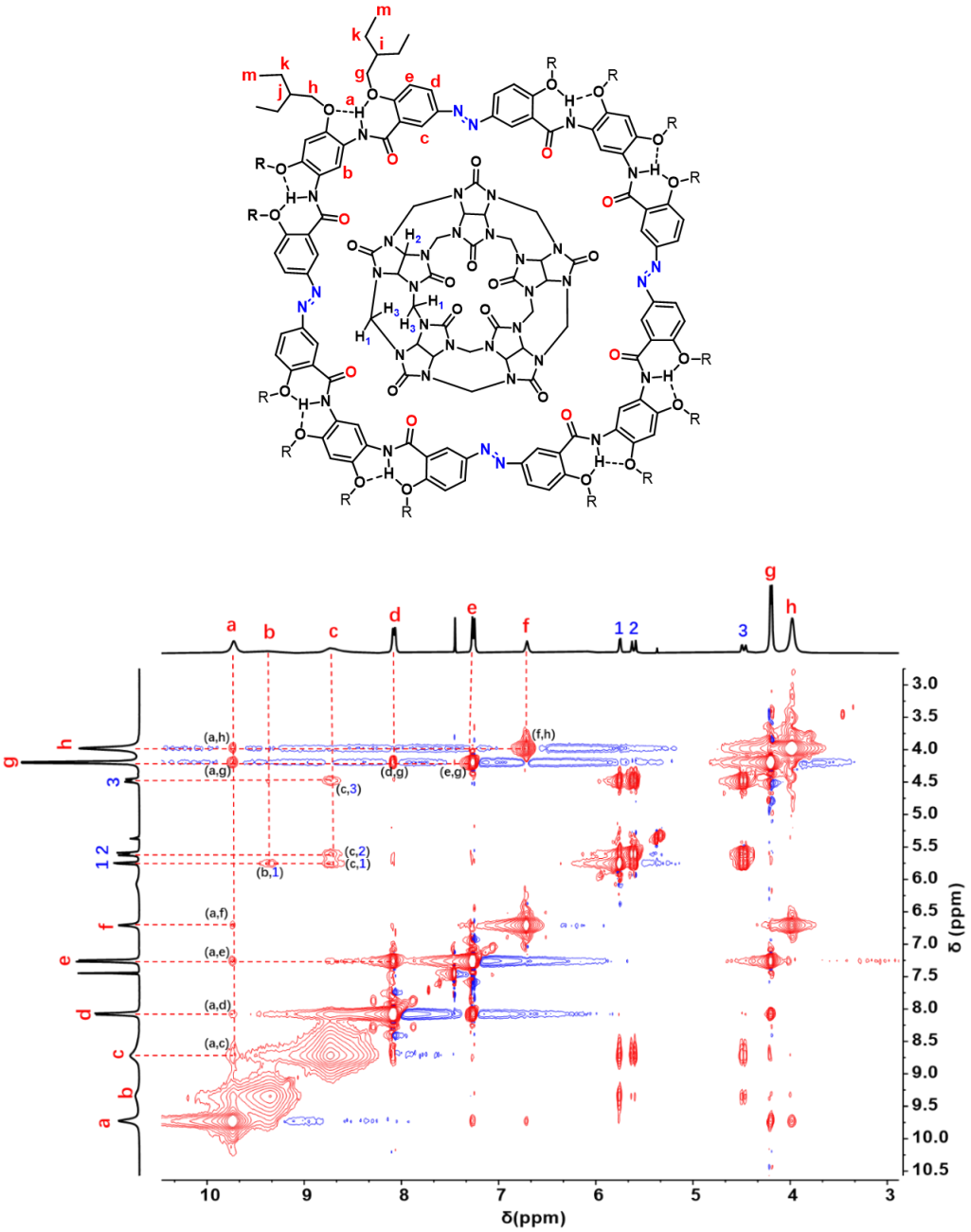

Figure S24. Expanded 2D NOESY spectrum of **1**@CB[5] in the presence of 2 equiv. of $NaClO_4$ (10 mM in $CDCl_3/CD_3CN$, 2:1 v/v, 400 MHz, 298 K, mixing time = 0.4 s).

2D ROESY for H-G Interactions

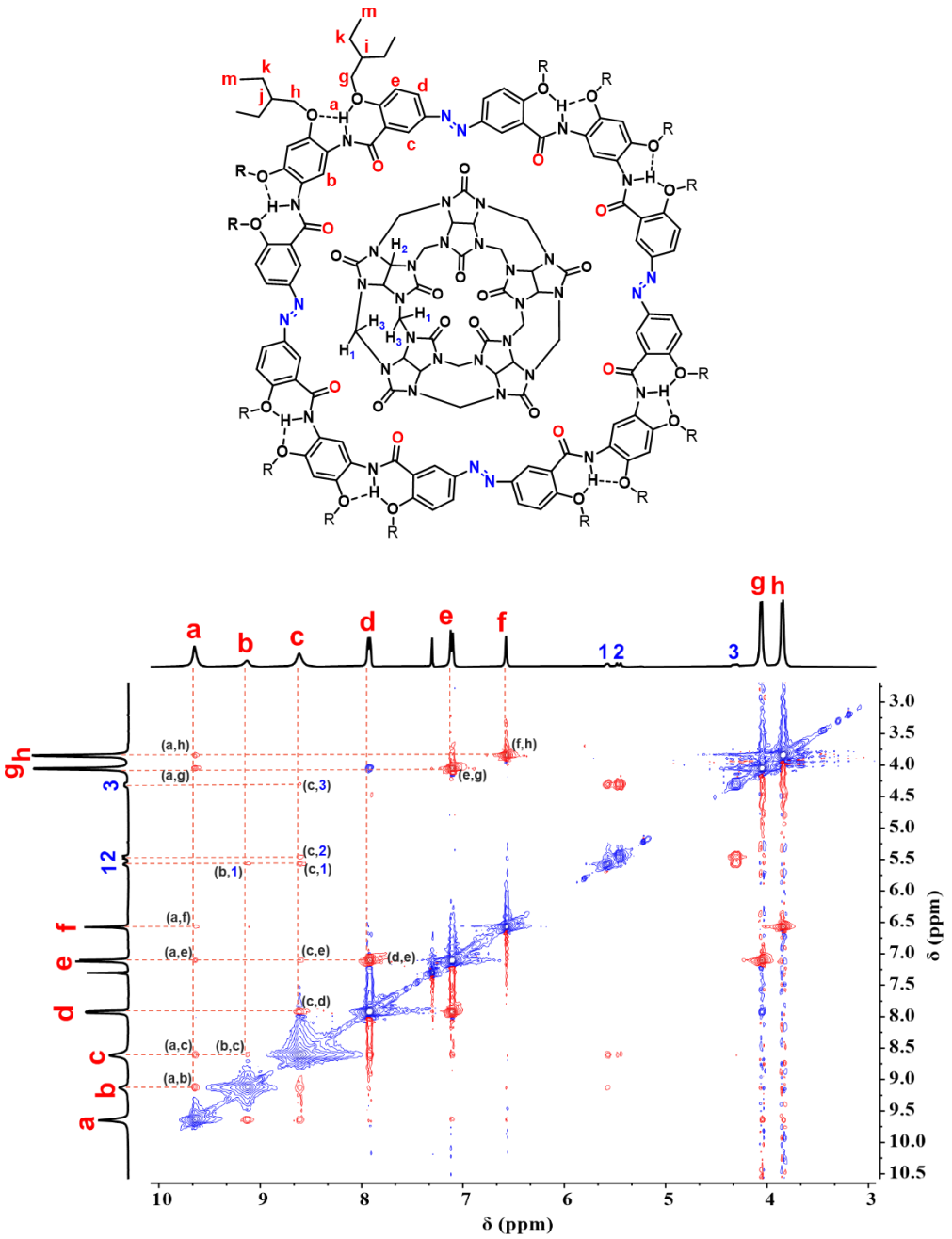

Figure S25. Expanded 2D ROESY spectrum of **1**@CB[5] in the presence of 2 equiv. of $NaClO_4$ (10 mM in $CDCl_3/CD_3CN$, 2:1 v/v, 400 MHz, 298 K, mixing time = 0.4 s).

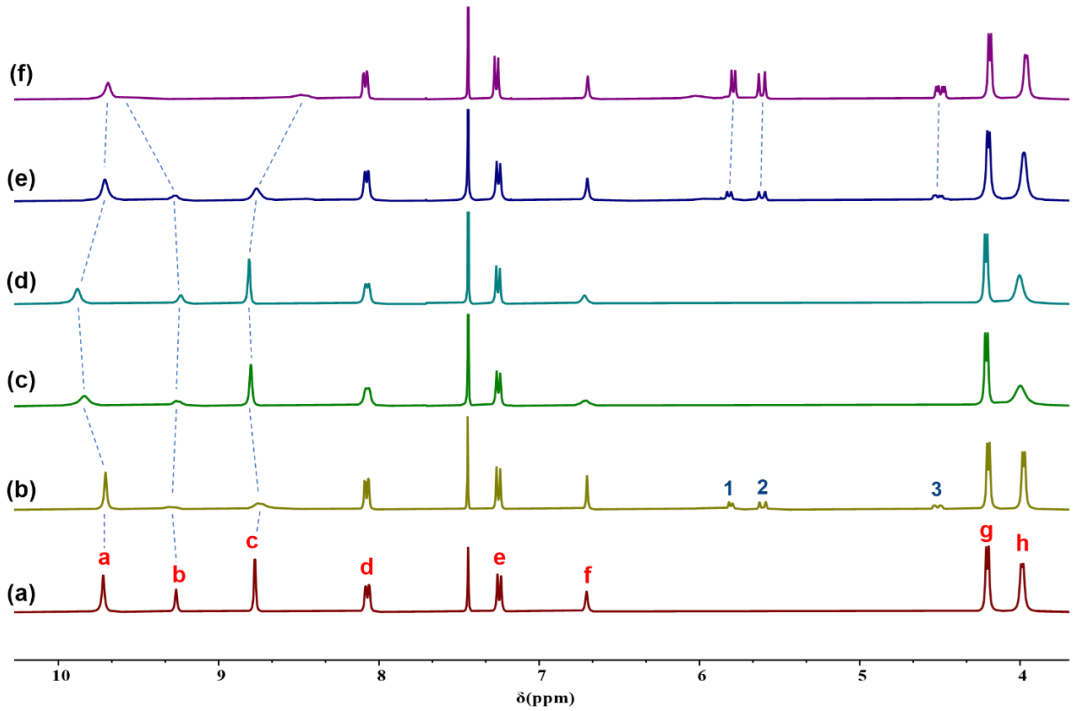

Figure S26. ^{1}H NMR spectra (2 mM in $CDCl_3/CD_3CN$, 2:1 v/v; 400 MHz; 298 K) of (a) macrocycle **1**, (b) **1**@CB[5], (c) **1** with 1 equiv. of $NaClO_4$, (d) **1** with 2 equiv. of $NaClO_4$, (e) **1**@CB[5] with 1 equiv. of $NaClO_4$, and (f) **1**@CB[5] with 2 equiv. of $NaClO_4$.

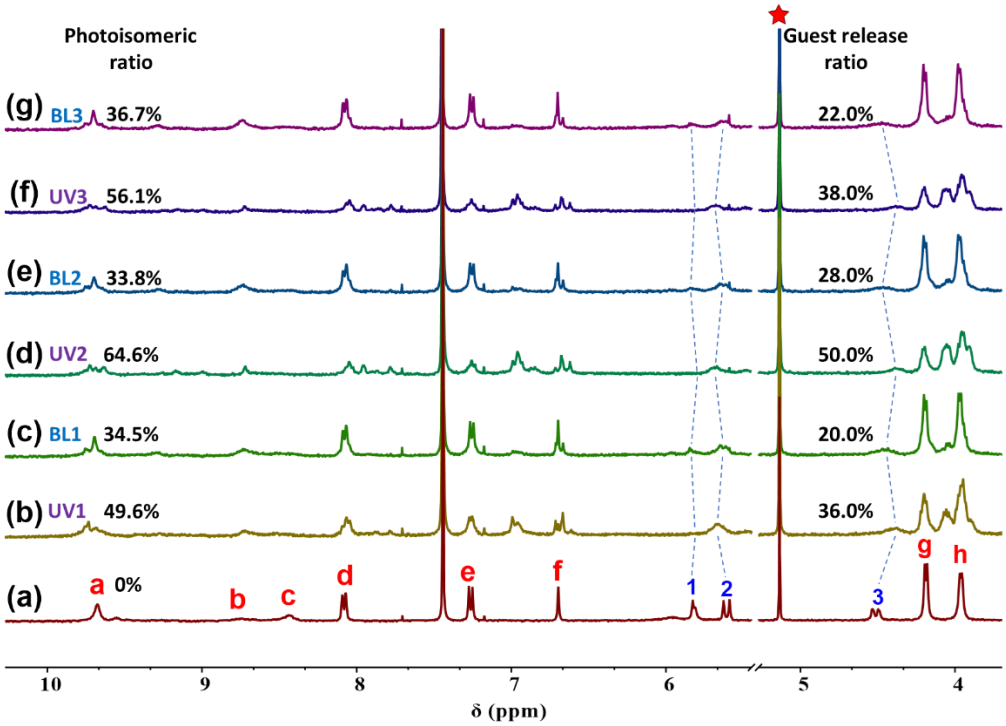

Figure S27. ^{1}H NMR spectra ($CDCl_3$/CD_3CN, 2:1 v/v; 400 MHz; 298 K, [**1**]= 0.5 mM) illustrating reversible host–guest binding and release during repeated photo-cycling, (a) **1**@CB[5] in the presence of 2 equiv. of $NaClO_4$ (initial state); (b, c) the first photocycle, (d, e) the second photocycle; and (f, g) the third photocycle. Photoisomeric ratios and guest-release ratios were determined based on the integrals of proton *e* of macrocycle **1** and proton *3* of CB[5], using 1,3,5-trioxane as an internal standard (*marked by a red star).

2D DOSY Spectrum

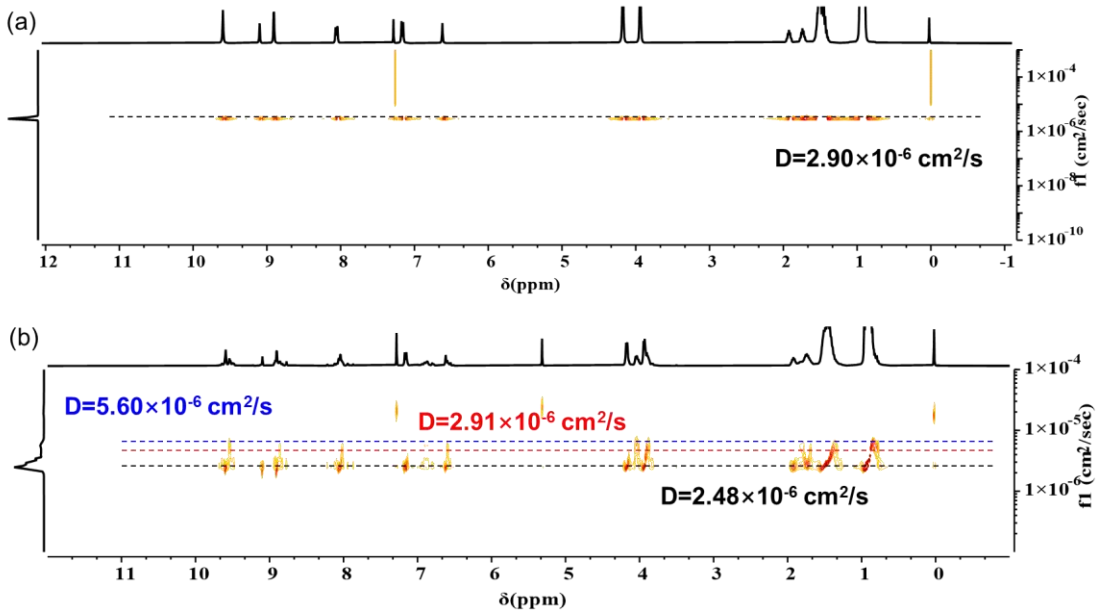

Figure S28. 2D DOSY spectrum of macrocycle **1** (10 mM, 400 MHz, $CDCl_3$, 298 K) recorded (a) before UV irradiation (b) after UV irradiation.

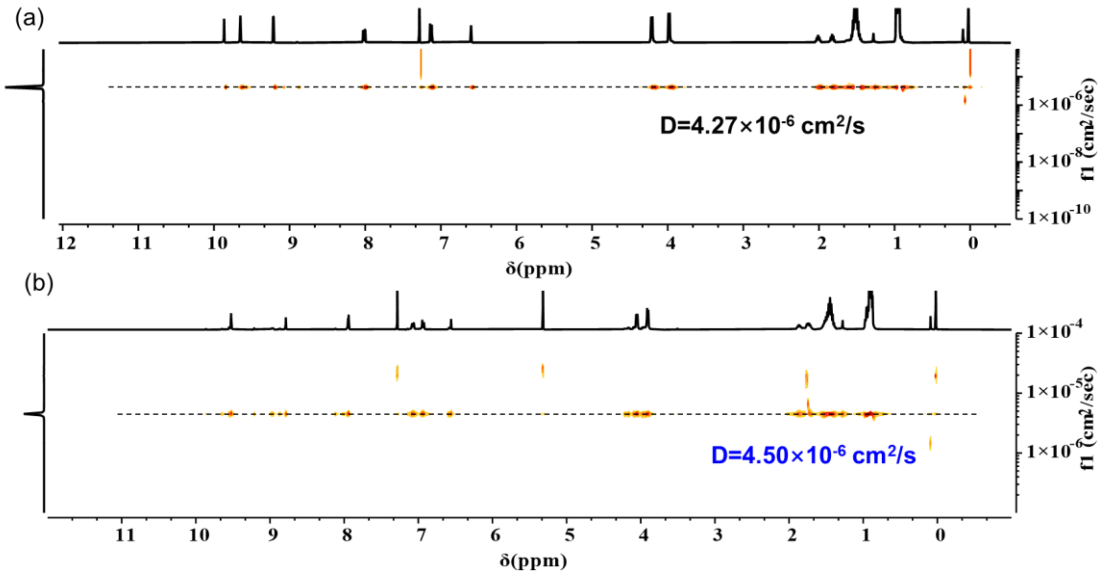

Figure S29. 2D DOSY spectrum of macrocycle **2** (10 mM, 400 MHz, $CDCl_3$, 298 K) recorded (a) before UV irradiation (b) after UV irradiation.

Hydrodynamic radius of macrocycle can be estimated using the Stokes-Einstein-Sutherland equation[3]:

$$r = \frac{\kappa_B T}{6\pi\eta D}$$

where κ_B is the Boltzmann constant, T is the absolute temperature, η is the viscosity of solvent, and D is the diffusion coefficient. The hydrodynamic radius of macrocycle **1** before irradiation ($r_{\mathbf{1}(\text{before UV})}$) can thus be obtained:

$$r_{\mathbf{1}(\text{before UV})} = \frac{\kappa_B T}{6\pi\eta D} = \frac{1.38\times10^{-23}\times298.15}{6\times3.14\times5.42\times10^{-4}\times2.9\times10^{-10}} = 1.39 \text{ nm}$$

Similarly, following the same method, the data presented in the following table were calculated.

Table S3. Hydrodynamic radii of macrocycles

Macrocycle	r_1 (nm)[a]	r_2 (nm)[b]
1	1.39	0.72, 1.38, 1.90
2	0.94	0.90

From the calculation results, it can be concluded that macrocycle **1** exhibits a significant change in radius before and after UV irradiation, as well as a substantial alteration in shape and size. This indicates that a portion of the CB[5] molecules are released from the macrocycle **1** upon UV irradiation, which is consistent with the experimental observations. [a] Hydrodynamic radius of macrocycle prior to UV irradiation. [b] Hydrodynamic radius of macrocycle after UV irradiation.

References

[1] Z. Ye, Z. Yang, L. Wang, L. Chen, Y. Cai, P. Deng, W. Feng, X. Li and L. Yuan, A dynamic hydrogen-bonded azo-macrocycle for precisely photo-controlled molecular encapsulation and release, *Angew. Chem. Int. Ed*., 2019, **58**, 12519-12523.

[2] A. D. Becke, Density-functional thermochemistry. III. The role of exact exchange, *J. Chem. Phys.* 1993, **98**, 5648-5652.

[3] H. Wu, Y. Wang, L. Đorđević, P. Kundu, S. Bhunia, A. X-Y. Chen, L. Feng, D. Shen, W. Liu, L. Zhang, B. Song, G. Wu, B-T. Liu, M. Y. Yang, Y. Yang, C. L. Stern, S. I. Stupp, W. A. Goddard III, W. Hu and J. F. Stoddart, Dynamic supramolecular snub cubes, *Nature*, 2025, **637**, 347-353.